INSIGHTS-JOURNAL OF
LIFE AND SOCIAL SCIENCES

INSIGHTS-JLSS
Insights-Journal of Life and Social Sciences

FABRICATION AND EVALUATION OF IONICALLY CROSS-LINKED TRAGACANTH GUM NANOCOMPOSITES FOR THE DELIVERY OF ANTI-CANCER DRUGS

Original Article

Hafiz Muhammad Bilal[1], Muhammad Saeed[2], Muhammad Shahzad[3], Meryem Mehmood[4], Muhammad Bilal[5], Areej Safdar[6], Areeba Musferah[7], Ayesha Ajmal[8], Shazia Aslam[9], Safdar Ali[10]*

[1]Faculty of Rehabilitation and Allied health Science (FRAHS), Riphah International University, Lahore, Pakistan.
[2]Mohi-ud-Din Islamic Institute of Pharmaceutical Sciences, Mirpur AJ & K, Mohi-ud-Din Islamic University, Nerian Sharif, AJ & K, Pakistan.
[3]Department of Pharmaceutical Sciences, Gomal University, Dera Ismail Khan, Pakistan.
[4]Faculty of Rehabilitation and Allied health Science (FRAHS), Riphah International University, Al Mizan Campus, Rawalpindi, Pakistan.
[5]Department Microbiology and Molecular Genetics, Bahauddin Zakariya University, Multan, Pakistan.
[6]Department Microbiology and Molecular Genetics, The Women University, Multan, Pakistan.
[7]Department of Pathology, Faculty of Veterinary Science, Cholistan University of Veterinary and Animal Sciences, Bahawalpur, Pakistan.
[8]Department of Veterinary and Animal Sciences, Muhammad Nawaz Shareef University of Agriculture, Multan, Pakistan.
[9]Department of Chemistry Education, Universitas Negeri Yogyakarta, Indonesia.
[10]Department of Microbiology, Cholistan University of Veterinary and Animal Sciences, Bahawalpur, Pakistan.

Corresponding Author: Safdar Ali, Department of Microbiology, Cholistan University of Veterinary and Animal Sciences, Bahawalpur, Pakistan, safdarali5065012@gmail.com

Conflict of Interest: None

Grant Support & Financial Support: None

Acknowledgment: We acknowledge the valuable support of the research and laboratory staff involved in the synthesis, characterization, and biological evaluation of the TG-CS nanocomposites.

ABSTRACT

Background: Nanoparticle-based drug delivery systems have gained significant attention due to their ability to provide sustained release, localized drug administration, and advanced diagnostic capabilities. Chitosan-based drug-loaded nanoparticles (CSNPs) are particularly promising for targeted and controlled drug delivery, as well as imaging applications.

Objective: This study aimed to develop nanocomposites for the delivery of the anticancer drug methotrexate (MTX) using a cross-linked chitosan (CS) and Tragacanth Gum (TG) system via ionotropic gelation. The physicochemical properties, drug release kinetics, and biocompatibility of the formulations were evaluated.

Methods: TG-CS nanoparticles were synthesized and characterized using UV-visible spectroscopy, FTIR, SEM, and EDX. Particle size, polydispersity index (PDI), and zeta potential were measured. Four formulations (NP1-NP4) were prepared, and their loading capacity (LC), entrapment efficiency (EE), and yield were assessed. In vitro drug release kinetics were analyzed, and cytotoxicity was evaluated via MTT assay on HEPG-2 and MCF-7 cell lines. Hemolytic activity was also examined.

Results: The nanoparticles exhibited an absorption peak at 400 nm (UV-vis) and an N-H stretch at 3477 cm^{-1} (FTIR). NP3 demonstrated optimal properties with a particle size of 250 nm, PDI of 0.571, and zeta potential of 80.5 mV. It showed the highest EE (75.9%), LC (9.35%), and yield among all formulations. Drug release followed the Korsmeyer-Peppas model with first-order kinetics. NP3 exhibited greater hemolytic activity (185%) due to saline compatibility, whereas NP2 showed negligible impact (2.5%).

Conclusion: The TG-CS nanocomposite (NP3) proved to be an effective sustained-release carrier for MTX, with high biocompatibility and anticancer potential. These findings highlight its promise for targeted drug delivery in cancer therapy.

Keywords: Tragacanth Gum, Nanocomposites, Drug delivery, Anti-Cancer, TG-CS, FTIR.

INTRODUCTION

A broad variety of diseases that can affect any part of the body is cancer, also known as neoplasms malignant tumors. Cancer is characterized by rapid proliferation of abnormal cells and invasion into other body regions, causing metastasis, which proves to be the primary cause of fatalities [1]. Nearly eight million cases per year reported from economically underdeveloped nations account for 82 percent of global cases [2]. As a result of menopausal hormone therapy, greater screening, and changes in reproductive factors, it was observed that the incidence rates of breast cancer in Western countries reached a peak of about 30 percent [3]. In Pakistan, 8.6% (2.1 percent globally) of all new cancer cases and 7.2 percent (1.8 percent globally) of all cancer fatalities are due to lip and oral cavity cancer. Nearly 66.4 percent of all lip and oral cavity cancer cases and 77.2 percent of fatalities from this malignancy occur in less developed nations [4]. Taken as a whole cancer radiation therapy survival rates have grown in case of particular tumors, for instance tumor in head and neck, from about 30% two decades ago to about 80% now [5].

The therapeutic intervention of cancer knows several types such as immunotherapy, chemotherapeutics, surgical removal of tumors, and radiotherapy. Taken as a whole cancer radiation therapy survival rates have grown in case of particular tumors, for instance tumor in head and neck, from about 30% two decades ago to about 80% now [5]. Effective radiotherapy reflects how to maximize the capacity to kill cancer cells while staying within the range of tolerable doses that nearby healthy tissues may bear from radiation damage [6]. Immunotherapy is a breakthrough treatment for malignancies that don't respond to traditional medications. However, immunotherapy might be less successful in cancer patients with immunosuppression. Cancer immunotherapy effectiveness is found to be inversely correlated with tumor burden [7].

In many malignancies, unpredictable toxicity and efficacy of the therapy frequently become barriers to effective immunotherapy. Patients with various cancer types and stages have shown varying responses to the same treatment [8]. A variety of delivery systems, including microspheres, polymer implants, liposomes, proteins, polymers, and nanoparticles, have been developed and evaluated in both animal models and clinical studies [9]. A type of cancer treatment known as hormone therapy involves the removal, blocking, or addition of hormones to the body. The term "endocrine treatment" is also used. Stopping the body from producing a hormone and altering the way a hormone behaves in the body both impede the binding of a hormone to cancer cells. By using hormone therapy various cancers are treated such as [10]. Because of their enormous surface-to-volume ratios, which enable surface modification and the display of many surface functional groups like ligands, nanoparticles are advantageous for use in therapeutic applications [11]. However, the mononuclear phagocyte system quickly opsonizes and substantially clears the surface-unmodified nanoparticles [12].

Therefore, the ability to shield medications from gastrointestinal tract degradation, which causes the pharmaceuticals to deliver in diverse areas of inflammatory sites, is increased by the construction of nanomaterials with polymers generated from natural or synthetic origins[13]. Currently, bio-polymeric nanocomposites are of great interest in drug delivery as they illustrate superior biomedical characteristics [14] [15]. Most bio-polymeric nanocomposites are suitable drug carriers as they display highly improved properties in comparison to their related pure polymers [16] [17] [18]. The synthesis of cost-effective antibacterial nanoparticles (NPs) and their nanocomposites has been of substantial interest in numerous pharmaceuticals, biomedical, cosmetics, drug delivery as well as antimicrobial applications [19] [20] [21] [22].

Nano capsules containing plant extract were created using the micro-emulsion process and tragacanth gum (TG). Using an ultrasonic and magnetic stirrer, the impact of various parameters on the average size of manufactured nano capsules containing calcium chloride and aluminum was examined. When various nano capsules were tested for their antimicrobial effectiveness against E. coli, S. aureus, and Candida albicans using the shake flask method, the results revealed a 100% microbial decrease after 12 hours of shaking [23]. Drug loading and release can be improved with the use of nanocarriers. TG or modified TG was combined with an enhancing agent to create nano carrier-based TG. Amphotericin B oral bioavailability was increased using a hybrid lecithin-TG mucoadhesive nanocomposite nanocarrier [24]. For the release of numerous medications, including diclofenac sodium, methotrexate, quetiapine, fluorouracil, Daucus carota, silymarin, naringin, ibuprofen, theophylline, and loperamide, others have created TG-based drug carriers [25]. Generally speaking, nanocarriers can be categorized as either organic, inorganic, or a combination of the two [26].

Micelles are organized aggregates and are amphiphilic molecules that self-assemble into (small surfactants and amphiphilic polymers). Due to their comparatively great physicochemical stability, micelles made of polymers with larger molecular weights are commonly utilized as nanocarriers. [27] [28]. A macromolecule with a heavily branched 3D structure is called a dendrimer. In general, it is composed of a central core, units that are repeatedly hyper branched, and a corona that contains functional groups [29]. The physicochemical characteristics of dendrimers are similar to those of other polymers, and they can mix with different active molecules to create products

[30]. When it comes to CNTs (carbon nano tubes), their hydrophobicity and ability to π – π stacking properties are determined by the composition of CNTs with sp2 carbon. As a result, substances containing aromatic rings can bind to the CNT surface. For instance, Chlorin e6 (Ce6), a heterocyclic aromatic compound having photosensitizing characteristics for photodynamic therapy, was reported as nanocomposites by [31]. Among the most prevalent raw ingredients in nature is polysaccharide gum. These bio-based materials are easily obtainable, reasonably priced, non-toxic, and environmentally benign because they are made from renewable resources. It is not unexpected that polysaccharide gums have a wide range of applications. For instance, the industrial use of polysaccharides in the United States is growing at a pace of 3% per year, or around three million tons per year. As a biomaterial, TG has been applied in the biomedical field as drug carriers and for wound healing, as well as in industrial applications including food packaging and water purification [32].

When a stem or root is injured, the soft gum is forced to be secreted and quickly dries on the trunk [33]. Tragacanth gum is naturally produced as bark exudate of *Astragalus gummifer*. It is also known as gum Katira or Katira in Iran and some other countries. A little woody evergreen shrub belonging to the Astragalus genus, which has over 2000 species, can be found in semi-desert and hilly regions of southwest Asia, including Pakistan, Iran, Turkey, Syria, and Greece. Its height is between 10 cm to 1.00 m [34]. Tragacanth has been credited in modern medicine as having antiviral and antibacterial properties [35]. For quicker healing of the wound, it is presumably capable of causing the myofibroblasts to contract [36].

A mucopolysaccharide linked to cellulose, chitosan is one. Chitin, the main component of crab exoskeletons, is deacetylated to produce chitosan. Rouget originally characterized it in 1859 and 1894, and Hoppe-Seyler gave it a formal name [37] [38] [39] [40] . For utilization of chitosan in various manipulations such as nanocomposites formation it is first modified chemically. One of the first generations of anticancer medications to employ a folic acid analog was methotrexate (MTX). Numerous cancers, including leukemia, hematologic malignancies, osteosarcoma, breast and cervical cancer, and even rheumatoid arthritis, can benefit from the usage of MTX [41]. In this regard, described the synthesis of chitosan-based nanoparticles (MTX-CS-NPS) that contain methotrexate as a model medication and include an amphiphilic made of amino acids that have pH-responsive characteristics (77KS) during the ionotropic completion process [42].

MATERIAL AND METHODS

The present research work was performed for the synthesis of methotrexate-loaded chitosan nanoparticles using the blend of TG polymer. All preparations for the solution were made in distilled water or other organic solvents. All the materials which were required for the synthesis of MTX loaded TG-CS nanoparticles and instruments were used for the characterization and evaluation of nanoparticles are shown in table 1.

Table 1: The list of instruments for synthesis and characterization of TG-CS nanoparticles

Instrument	***Company Name***
UV-visible Spectrophotometer	UV-1700 Pharmaspec Shimadzu, Japan
FTIR-spectroscopy	IR Prestige-21 Shimadzu, Japan
Hot plate and Magnetic stirrer	Topo MS300HS, M Tops,
Dynamic Light Scatter	Malvern, UK
Particle Size Analyzer	Zeta sizer Nanoseries Malvern, UK
Centrifuge Machine	Beckman, UK
Ultra sonicator	Sigma Aldrich
Balance Machine	PerciaXB120A
Scanning Electron Micros Joel	Joel JSM-IT100
pH Meter	Peak instruments INC, Houston
Microcentrifuge Machine	Sigma Aldhric

Lyophilizer	CHRIST alpha 1-4 LD, UK
Nylon syringe filters	Membrane Solution the USA
Chemicals	**Company Name**
Chitosan	Sigma Aldrich
Glacial Acetic Acid	Sigma Aldrich
Sodium Chloride	Sigma Aldrich
Acetone	Sigma Aldrich
Ethanol	Sigma Aldrich
Methotrexate (MTX, CAS no. 59-05-2)	Sigma Aldrich
Di-methylsulph-oxide (DMSO)	Sigma Aldrich
Sodium Hydroxide	Sigma Aldrich
Phosphate buffer, saline	Sigma Aldrich
Tragacanth Gum	Sigma Aldrich

METHOD

Selection and Plant Identification

The plant used for this research work was *Astragalus gummier*, the common name of this plant is Tragacanth Gum, also known as Gond Katira. The gum is obtained by exudation from the trunk and branches of *Astragalus gummier* in Pakistan [43]. The dried ribbon-like tragacanth was available in ground form, and it was purchased from a scientific store.

Preparation of Plant Extract

For the preparation of plant extract, the first stock solution of Glacial acetic acid (1%) was prepared by dissolving 1.00 mL Glacial Acetic acid in 100 mL distilled water, then 10 mg of TG powder was added to this stock solution. It was then allowed to stir for about 24 hours with a magnetic stirrer.

Physical Appearance

For physical evaluation such as color, texture, and odor gum powder were examined thoroughly.

Solubility and pH

To ascertain the solubility profile of the TG, a small amount of powdered TG was introduced to several solvents. A calibrated pH meter was used to measure the pH of the resulting suspension after adding 40 mg of gum powder to 100 mL of distilled water.

Estimation of carbohydrates

Various other tests were performed such as the Molisch's test, Iodine test, and Ruthenium test for the qualitative estimation of carbohydrates present in TG powder. For Molisch's test 2 mL of Molisch's reagent in 100 mg of dried TG powder and a few drops of concentrated sulfuric acid were added slowly. They noted the formation of color complex. The Ruthenium test was performed by taking a small quantity of dried gum powder, mount it on a slide with ruthenium red solution, and observe it under a microscope. For identification of polysaccharides, an Iodine test was performed on test sample in which 10 mg of dried mucilage powder was mixed in 1 mL 0.2 N iodine solution [19].

Methotrexate Loaded TG-CS Nanoparticles

For the formation of methotrexate nanoparticles, a previously published coacervation approach was slightly modified [119]. For this purpose, polymer solutions and methotrexate solution were prepared separately as mentioned below. Then by keeping the amount of drug constant four different formulations of polymers (chitosan and TG) were prepared as shown in table 2.

Preparation of anionic polymer solution

The Ionic gelation method was used for the synthesis of nanoparticles [20].

For the preparation of anionic polymer 2%, w/v solution of TG was prepared. For this purpose, 20 mg of TG was dissolved in 100 mL of distilled water, it was then continuously stirred on a hot plate by setting the parameters such as temperature kept at 60 0C for about one hour and stirring continued for about two days for complete desolation of TG. Utilizing 0.1 N HCL, the pH of this solution was brought down to 5.2 by dissolving 8.33 mL of concentrated HCL (0.1 N) in distilled water (1000 mL).

Preparation of cationic polymer

The cationic solution was prepared by dissolving chitosan in glacial acetic acid. It was made by mixing distilled water (99.9 mL) and glacial acetic acid (0.1 mL) until the mixture was homogeneous and contained 0.1% V/V. This acetic acid solution received 0.02 g of chitosan before being magnetically agitated into a homogeneous mixture. It contained 0.02 percent cationic polymeric solution. Using 1N NaOH, which was created by dissolving 40 g of sodium hydroxide in 1000 mL of water, the pH was adjusted to 5.5.

Preparation of methotrexate solution

0.01 g of methotrexate (MTX) was dissolved in 2 mL DMSO, and then gently added to the Chitosan solution with constant stirring at 3500 rpm speed.

Preparation of nanoparticle solution

For the preparation of nanoparticle solution ionotropic gelation was used, the plant gum solution TG was dropwise added to chitosan solution while it was continuously stirred at a hot plate. After this 10 mL of methotrexate solution was added and continued to stir for about one hour. The resultant solution was centrifuged at 12000 rpm for about one hour at 50C. Four different formulations were made by changing the concentration of methotrexate while the concentration of TG solution and chitosan was kept constant. The NP3 formulation was lyophilized and stored in a desiccator and other formulations were also made in the same way. The following table 2 shows the formulations

Table 2: Four formulations made for MTX loaded TG-CS nanoparticles

Formulation Code	TG Conc. (g)	Methotrexate Conc. (mL)	Chitosan Conc. (g)
NP1	0.02	0.02	0.01
NP2	0.02	0.04	0.01
NP3	0.04	0.02	0.01
NP4	0.03	0.04	0.01

Yield in Percentage (%)

From a pharmaceutical perspective, the percentage yield (%) of the nanoparticles created by a particular method is a crucial variable since it may be used to estimate the likelihood of industrial scale-up and the viability of a procedure. The highest yielding process is seen to be optimal. The percentage yield was estimated to assess the effectiveness of the production processes [53]. After lyophilization, (CHRIST alpha 1-4 LD, UK) the total amount of powder was measured using an analytical weighing scale (PerciaXB120A), and the percentage yield was estimated using the formula below.

Percentage Yield = $$\frac{Quantity\ of\ CNPs\ Obtained}{Total\ mass\ of\ all\ ingradents\ (Chitosan+TG+drug)} x100$$

Characterization of Nanoparticles

Different analytical techniques were used for the characterization of nanoparticles such as UV-Visible spectrophotometry, Dynamic Light Scattering (DLS), Scanning Electron Microscope (SEM), X-ray Diffraction Spectroscopy (XRD), Energy Dispersive X-ray Spectroscopy (EDS), and Fourier Transmission Infrared spectroscopy (FTIR).

UV-Visible Analysis

After centrifugation, pellets were collected to prepare the sample for UV-Visible analysis. The pellet was dissolved in 30 mL of distilled water in a glass vial to create a homogeneous mixture. Optical characteristics were determined using a UV-Vis spectrophotometer. For further dilution, 5 mL of the sample was taken from the stock and diluted in 30 mL of water. 3.00 mL of the diluted solution was collected for analysis. The blank reference was distilled water. Analysis of UV-Visible spectra in the 200-1000 nm range was done. And the adjusted wavelength was 450 nm.

Analysis using Fourier Transform Infrared Spectroscopy (FTIR)

Physical properties of MTX, chitosan, and TG, with a chosen NP3 formulation, after being grounded with KBr, the pellets were scanned over 400-4000 cm-1 were evaluated by using IR prestige-21 Shimadzu, Germany. To determine the compatibility and physiochemical interactions of the polymers, the FTIR spectra of the blank NPs were also collected.

Encapsulation Efficiency (EE) and Drug loading Capacity (LC)

Indirect calculations were used to determine entrapment efficiency (EE) and loading capacity (LC). To eliminate excess TG, chitosan, and un-capsulated drug, all formulations were spun in ultracentrifuge equipment at 12000 rpm for one hour at 5°C. With the help of What-man filter paper, the supernatant was collected, and the absorbance was measured using quartz cells with a 1.00 cm path length on a UV-1700 Pharma spec spectrophotometer (Shimadzu, Japan). The un-entrapped fraction of the drug was determined in the supernatant by employing a calibration curve of MTX solution at 304 nm in this approach. The LC and EE were determined by using the following equation

LC = $$\frac{\text{Total amount of drug added} - \text{Amount of drug untrapped}}{Total\ mass\ of\ CNP} x\ 100$$

EE = $$\frac{\text{Total amount of drug added} - \text{Amount of drug untrapped}}{Total\ amount\ of\ drug\ added} x\ 100$$

Particle Size, Polydispersity Index (PDI), and Zeta Potential Analysis

While PDI and zeta potential are markers of homogeneity and performance, the particle size of TG-CS NPs determines how effective they are at actively targeting cancer sites. Colloidal durability, accordingly. Zeta Sizer Nano (Zeta sizer Nano sizers Malvern, UK) was employed for the measurement of particle size, PDI, and zeta potential.

Scanning Electron Microscopic Studies

The morphology and surface properties of MTX-loaded TG-CS NPs were assessed using scanning electron microscopic (SEM). Over the metal stub, the lyophilized powder was positioned on a silicon chip with an electro-conductive surface (aluminum). The materials were coated on the stubs and studied using a 10kV electron acceleration voltage field emission scanning electron microscope (FESEM, JSM-5910, JEOL, and Japan) at various magnifications.

Powdered X-Ray Diffraction (PXRD) Analyses

PXRD analysis of MTX, chitosan, TG, the physical mixture including equal proportions of components, and the selected formulation (NP2) was done to determine the physical condition of the individual components. PXRD diffractometer (Bruker Axs, D8 Advance, Germany) with CuK radiation, 45kV monochromatic voltage, and 40 mA electric current was used to obtain the X-ray diffracto-gram based on Bragg's law. The 2-diffraction angle ranged from 10° to 60°.

In-Vitro Drug Release Studies

By conducting dissolution studies and using the kinetic modeling method, all formulations were assessed for their in-vitro release characteristics. To achieve this, prepared formulations containing 2 mg of MTX were ingested and dissolved in 2 mL of pH 7.4 phosphate buffer saline (PBS). This investigation employed a dialysis membrane (Spectrum®) with an 8–10 KDa cutoff value. Before starting the experiment, the membrane was immersed in distilled water for three hours to clear out all the pores. It was appropriately sized and then a formulation containing 2 mg of MTX suspended in PBS 7.4 was added. It was then placed in 600 mL of dissolve medium (PBS 7.4 with 0.5% tween 80 to maintain sink conditions) at 37±0.5 °C.

The study made use of a paddle apparatus of USP type II, with paddles rotating at a speed of 50 rpm. To maintain sink conditions, 3 mL samples were taken out at regular intervals, and the dissolving vessels were refilled with an equivalent volume of the new dissolution medium. The samples were collected, filtered via 0.45 µm Nylon syringe filters (Membrane Solution USA), and then examined using a UV-Spectrophotometer (UV-1700 Pharma spec Shimadzu, Japan) set to a maximum wavelength of ƛm 430 nm. To reduce inaccuracy, readings were obtained three times. The calculated cumulative percentage release was assessed for each sample using various kinetic models, such as the Higuchi and Korsmeyer-Peppas models, the zero-order, and first-order models [44].

Release Kinetic Models

Five distinct kinetic models were considered to suit the experimental data to explore the MTX release from the various types of NPs.

Zero-Order

This model was defined when n = 1 in Ritger-equation Peppa's and k_0 is a kinetic constant, and it is based on zero-order drug delivery [45].

$$\frac{Mt}{Minf} = K_{0t}$$

Where K0 represents kinetic constant.

First-Order

The following equation depicts first-order drug delivery.

$$\frac{Mt}{Minf} = \alpha\,[1- \exp(-bt)]$$

where a and b are the first-order rate constants, Only the initial 60 % of the drug release from the NPs is covered by the above-mentioned mathematical model.

Ritger-Peppas Equation

The third model is the Ritger-Peppas equation [46].

$$\frac{Mt}{Minf} = K_1 t^n$$

Where, Mt and Min f represent the cumulative drug release at time t and infinite time, respectively; k1 is a constant that depends on the structural and geometrical properties of the particles; t represents the release time; and n represents the diffusiona1 exponent, which defines the drug release mechanism. The Fickian diffusion is the drug release mechanism for spherical delivery systems when n = 0.43. When n = 0.85, Case II transport constitutes the entire drug release mechanism [46].

Higuchi Model

The fourth model is the Higuchi model. The transport mechanism of spherical hydrogel systems can also be studied using this model, which is commonly used to characterize the drug transport mechanism of thin film hydrogels.

$$\frac{Mt}{Minf} = K_H t^n$$

Where, t is the release time and kH is a kinetic constant.

Peeps-Sahlin Model

Model 5 is based on the Peppas-Sahlin equation (Peppas and Sahlin),

$$\frac{Mt}{Minf} = K_1 t^n + K_2 t2^m$$

Where m is the diffusional exponent and k1 and k2 are kinetic constants.

Hemolysis

To analyze the hemolysis of nanoparticles, 4.00 mL of sterile human blood was taken from the University Medical and Diagnostic Centre (UMDC) lab. Red blood cells and serum were isolated from the blood by centrifuging it at 3000 rpm for 10 minutes. PBS (pH 7.4) was used to wash (RBC) pellets three times.

The obtained RBCs were diluted 10 mL of the formulation (0.5 mL, 1.00 mL, 2.5 mL and 5 mL) was vortexed with PBS (2.00 mL). 1.00 mL RBC suspension then centrifuged at 3000rpm for ten minutes. Saline and deionized water (10 mL each) were used as the positive and negative controls, with 1.00 mL of RBC suspension added as the final step. A UV spectrophotometer was used to measure the absorbance of the supernatant at 540 nm. For the calculation of % Hemolysis following equation was used

$$\% \text{ Hemolysis} = \frac{SA-NA}{PA-NA} x100$$

Where SA is sample absorbed PA is absorbed by positive control and NA is absorbed by negative control.

Statistical Analysis

For the statistical analysis (n=3), the one-tailed t-test was used. Studies on % yield, entrapment efficiency, loading capacity, particle size, PDI, and zeta potential were all subjected to statistical analysis. The p values were determined to see how different TG concentrations affected the NPS (NP1-CNP4).

Results and Discussion

The synthesis of methotrexate-loaded chitosan nanoparticles and their characterization utilizing UV-visible analysis, FTIR (Fourier transform infrared spectroscopy), DLS (Particle size and Distribution), SEM (Scanning Electron Microscopy), and EDS are both described in detail in this chapter (Energy Dispersive X-ray Spectroscopy). These are the following:

Physiological Evaluation of TG

Gum powder made from ribbon is white to light yellow in color, odorless and has an insipid, mucilaginous taste. The flakes vary from yellow to brown to give cream to tan powders in color. Both ribbon and flake gums are available in a variety of particle sizes and viscosities depending on the end use [47]. The major component of TG was D-galacturonic acid-containing branching acidic hetero-polysaccharides. After hydrolysis, other sugars are created, such as D-galactose, L-fucose (6-deoxy-L-galactose), D-xylose, and L-arabinose. With a predominance of D-galacturonic acid methyl ester rather than other compounds, bassorin (arabinogalactan) appears neutral [15]. Because of its hydrophilicity, this polysaccharide retains strength over a broad pH range and efficiently absorbs water. It is safe to consume orally because it is biocompatible and biodegradable. Since its major constituents are carbohydrates and sugar varying tests based on carbohydrate analysis were performed such as chromatography to evaluate its physiological properties. Table (3) represents a list of some analyses performed to characterize the physiological analysis of TG.

Table 3: Evaluation of different results used for physiological evaluation of TG

Test	Observation	Inferences
Molisch's test	The violet-green color observed at the junction of the two layers	Carbohydrate present
Ruthenium test	Pink color develops	Gum present
Iodine test	No color observed in the solution	Polysaccharides present (Starch is absent)

Solubility and pH

Tragacanth solutions are naturally slightly acidic. 1% solution was made by adding 1g of TG and 99 mL distilled water its pH was found within 5-6. It was most stable at the pH range from 4 to 8. Also, it showed good stability at 2 pH. Hence it was proved to be most acid-resistant gums

TG swells rapidly in either cold or hot water to form a viscous colloidal solution, which acts as a protective colloid and stabilizer. While it is insoluble in alcohol and other organic solvents, gum can tolerate small amounts of alcohol or glycol. The gum solution is fairly stable over a wide pH range down to extremely acidic conditions at about pH 2.The TG structure has a lot of carboxylic groups, hence the solubility of this substance fluctuates with ionic strength and pH levels, with the highest solubility occurring between pH 5 and 6 [48]. With diminishing concentration, TG solutions become less viscous, the decrease in PH occurs due to ionic dissociation of the carboxylic groups. According to research on the water absorption capabilities of different gums from 20 to 65 0C, TG has a better water absorption capacity than guar gum and locust bean gum. TG has varying hygroscopic characteristics caused by the acidic and ionic units in its chemical structure. It was discovered that the kind of initiator, monomer and crosslinking agent used for the synthesis had an impact on water absorption when a TG-based superabsorbent with water absorbency equivalent to 864 g water/g absorbent was examined [49].

Preparation of Polymeric Nanoparticles

For the preparation of TG-CS Polymeric nanoparticles, ionotropic gelation was used. This method depends upon the cross-linking the complexions between oppositely charged macromolecules that has been used to make CS nanoparticles. A polyanion, TG, is made to interact with cationic CS. It was made by adding CS droplets to a TG solution. To get the cation of CS, CS was dissolved in an aqueous acidic solution in the ionic gelation process. The polyanionic TG solution was continuously stirred and then it was added dropwise in chitosan solution. It was possible to create cross-linked chitosan nanoparticles by reacting negatively charged phosphoric ions from TG with the abundant NH3 group found in chitosan molecules. Water was extruded from the particles during the cross-linking and hardening processes, which may aid to prolong the drug release [50] When the nanoparticles were prepared, different types of phenomena were seen such as solution appearance, aggregation, and opalescent suspension. The last step signifies the end of the procedure.

Advantages of Ionotropic Gelation Method

The main advantage of ionotropic gelation was its irreversible physical cross-linking by electrostatic contact instead of chemical cross-linking which prevents potential reagent toxicity and other negative consequences. The approach was relatively affordable and straightforward. It also takes less time and equipment. Using no organic solvents.TG-CS nanoparticles' sole drawback is their lack of mechanical strength.

CHARACTERIZATION OF NANOPARTICLES

UV-Visible Spectrometric Analysis

UV-Vis Spectrophotometry is used for the determination of optical properties of synthesized TG-CS nanoparticles. It confirms the synthesis of TG-CS nanoparticles. TG-CS nanoparticles appeared to have an absorption peak of around 500nm shown in (Figure 2).

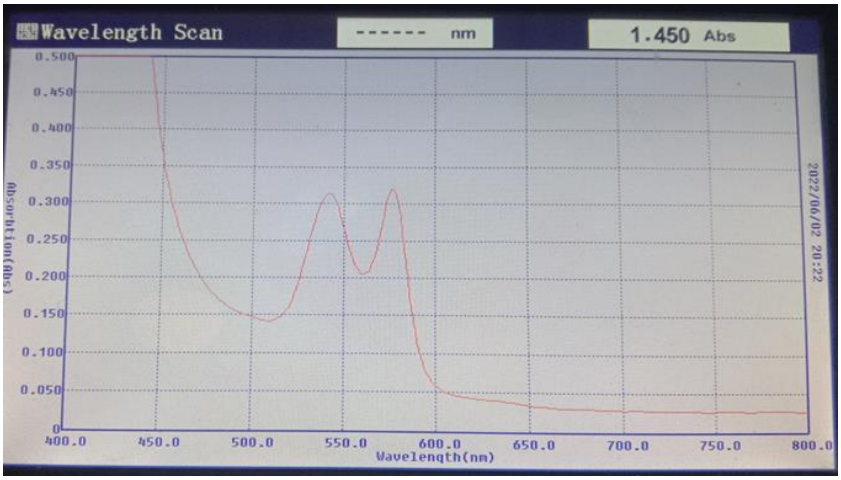

Figure 1: Present the UV visible spectrometric of TG-CS nanoparticles

FTIR Analysis

The FTIR spectrum of TG-CS displayed distinctive peaks at 3477 cm-1, replicating the N-H stretching of alkanes, 2990 cm-1, the C-H stretching of MTX, 1713 cm-1, the C=O stretching of MTX, 1490 cm-1, and the C-N stretching vibration, at 1246 cm-1 (Figure 2).

The distinctive peaks of chitosan were found at 3296 cm-1, which showed the stretching vibration of -OH groups, 1644 cm-1, which described the C=O of the acetamide group, 47, 48, 1526 cm-1, which represented the -NH bending vibration of the NH2 group, and 1063 cm-1, which demonstrated the stretching vibration of -CN and -CO.

The characteristic absorption bands in the FTIR spectrum of TG (Figure 2) correspond to the stretching vibrations of the hydroxyl (-OH) and carbonyl (C=O) groups, respectively, and are located at 3415 cm-1, 1750 cm-1, and 1640 cm-1. The stretching vibrations of the methylene (-CH2) group were attributed to the absorption bands at 2937 and 2867 cm-1, respectively. Additionally, there was a relationship between the absorption bands at 1244 and 628 cm-1 and the stretching vibrations of the C-O of the polyol and ether groups and the pyranose ring, respectively in (Table 3).

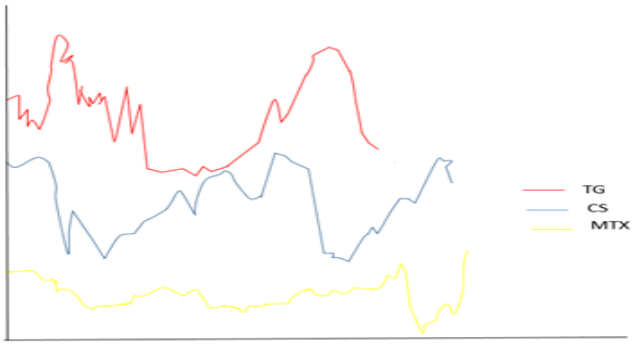

Figure 2: Depicts FTIR spectra of TG, CS, and MTX

Table 4: FTIR spectra of Chitosan and FTIR results of TG-CS nanoparticles

FTIR spectra of Chitosan		**FTIR results of TG-CS nanoparticles**	
Wave Number cm^{-1}	Functional Group	Wave Number cm^{-1}	Functional Group
3616	-OH stretch	3415	-OH stretch
2316	-COOH	1751	-COOH
2115	C Stretch	2867	C c Stretch
1646	C=C stretch	1646	C=C stretch
1042	C-O	1300	C-O
1515	N-H band	1100	N-H band

Encapsulation Efficiency, Percentage Yield, and Loading Capacity

The loading efficiency of the chitosan-TG nanoparticles ranged from 7.88% to 9.35%, while the efficiency ranged from 56.39% to 72.73%. Before raising the TG concentration to a particular level, CNP3, which corresponds to optimal ionic gelation of the components, entrapment effectiveness was directly related to the concentration of TG. Above this point, entrapment efficiency dropped due to the relative rivalry between the TG and MTX within the nanoparticles and the thickening of the shells brought on by the TG concentration. The protein that was enclosed in CNPs showed a comparable response. The loading efficiency and entrapment efficiency were reduced by raising drug concentrations. The main reason the NP1 had low EE was that the TG and CS concentrations were too low for encapsulating bigger amounts of the drug, whereas the NP2 had high chitosan volume but the EE calculated was still lower, showing low chitosan encapsulation capacity. The maximum drug content was encapsulated in NP3, demonstrating that the amount of methotrexate encapsulated increases with the amount of TG utilized. However, NP4's percentage is lower than NP3's because of low TG content, but NP1 and NP2's percentages are both lower than NP4's as shown in (Table 4)

Table 5: The entrap efficiency and loading capacity of all the formulations

Formulation code	**Entrapment Efficiency**	**Loading Capacity**	**Percentage of loaded Drug**	**%Yield**
NP1	65.5	9.03	81	70
NP2	70.8	9.02	72	65
NP3	75.9	9.354	95	75
NP4	69.23	7.88	83	72

Particle Size, Polydispersity Index (PDI), and Zeta Potential Analysis

The study revealed that the size range of 200nm to 300nm was regarded best to cross biological barriers also the size range up to 400nm was acceptable Sizes as small as 450 nm are also thought to be appropriate. According to a study, the ideal size range for Cs is 100-500 nm [51]. Particle sizes of the produced CNPs in this work were in the Nano-size range (200 nm to 409.8 nm) and met the criteria for improved antitumor effectiveness. Because raising the concentration of CS results in larger particle size ($p > 0.05$), it has been discovered that the size of nanoparticles is directly related to the variable ratio of chitosan. The DLS results were carried for both blanks as well as for drug-loaded which show peaks at range which exhibit in (Figure 3). Excellent colloidal stability is indicated by a zeta potential value greater than 30 mV; the positive potential is brought on by the positively charged chitosan found in CNPs. The results show that raising the CS concentration causes a drop in the zeta potential value which was 8.31 shown in (Table 5).

Table 6: Exhibit particle size, Zeta potential and PDI of all formulations with varying concentration of chitosan.

Chitosan (mg/mL)	Particle Size (nm)		Poly-dispersity Index		Zeta-potential (mV)	
Concentrations	Drug loaded	Without drug loaded	Drug Loaded	Without drug loaded	Drug loaded	Without drug loaded
1.0	290.2	200	0.39	0.218	86.1	8.31
2.0	305.1	291	0.456	0.399	574.8	556.9
3.0	321.5	358.6	0.495	0.418	652.4	563
4.0	409.8	462.5	0.554	0.571	655.6	596

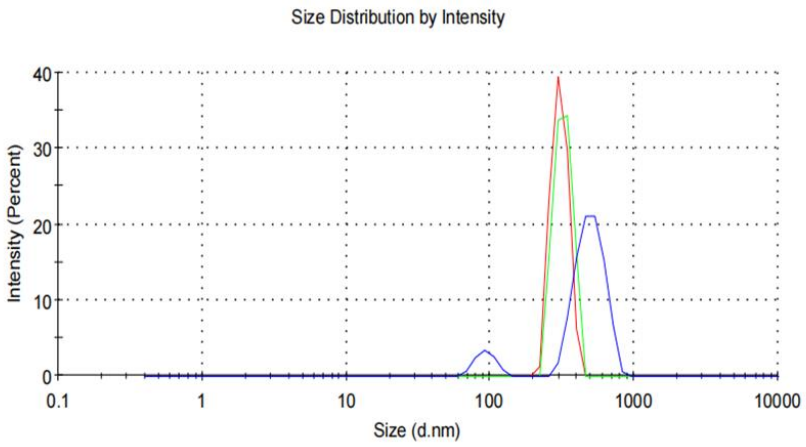

Figure 3: DLS result of MTX loaded TG-CS nanoparticle

Scanning Electron Microscopy

Figures display the produced nanoparticles' SEM picture. The crystal structure of the nanoparticles is revealed via scanning electron microscopy. CS and TG rough surfaces were visible in the SEM images (Figure A) (Figure B). Additionally, particles were seen in the TG SEM pictures. Figure C shows that drug precipitates are crystalline deposits, whereas Nano-formulation (NP3) is cubic in shape (Figure D). TG (X1000), CS (X22, 000), and operational voltage (20 kV) were used for SEM images, while 30 kV was used for images of drug precipitates (X7000) and nanoparticles, all shown in (Figure 4 & 4.1).

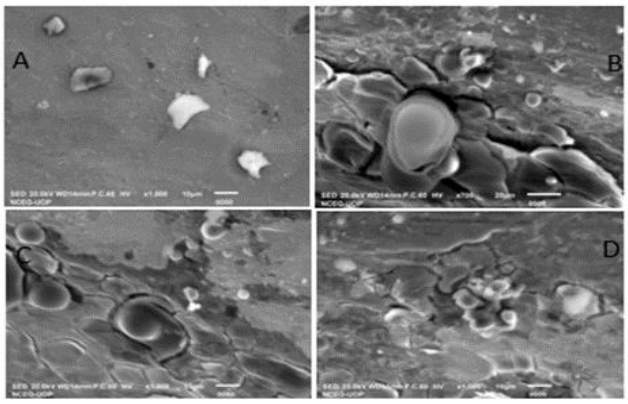

Figure 4: SEM results of MTX loaded TG-CS nanoparticles. The morphology of MTX loaded TG-CS nanoparticles A

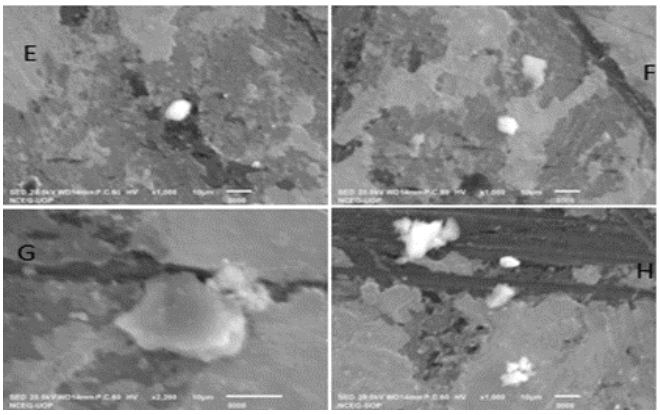

Figure 4.1: SEM results of Chitosan depict the crystalline morphology of MTX loaded TG-CS nanoparticles

Energy Dispersive X-Ray Micro Analysis (EDX)

The Energy Dispersive X-ray (EDX) Microanalysis is an elemental analysis method used in conjunction with electron microscopy that relies on the production of distinctive X-rays to identify the presence of elements in the specimen [52]. The EDX analysis of TG-CS nanoparticles reveals the presence of certain metal ions such as Cu, Na, Ca, Al and K. From the spectra it is that the highest content of Al was present shown in (Figure 5)

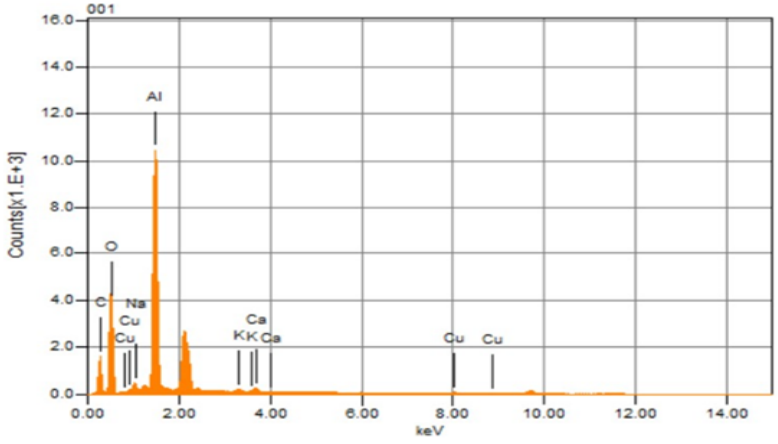

Figure 5: EDX results of MTX loaded TG-CS nanoparticles showing the trace amount of Cu, Na, K and maximum amount of Al.

In-Vitro drug Release Studies and Kinetic Modelling

Drug release over the course of the research, which lasted 24 hours, ranged from 50.3% (CNP4) to 70.1% (CNP3), indicating a continuous release pattern. Due to the quick release of surface-entrapped MTX, the drug was released more quickly at first, followed by a second persistent release phase. Due to chitosan swelling and hydration, the final slower release phase may correspond to the release of MTX from the core. Since the Korsmeyer-Peppas model exhibits higher correlation coefficient values, it was determined that the release of MTX from CNPs largely matched this model. Similar outcomes of the drug release mechanism have already been observed. The comparison of drug release studies of all formulations is shown in (Table 6).

Table 7: Kinetics mechanics followed by the formulations with the most acceptable Korsmeyer peeps kinetics

Formulation	Zero-order		First Order		Higuchi Kinetics		Hixon Kinetics	Crowell	Korsmeyer peppas Kinetics	
NPs	R^2	K_0	R^2	K_0	R^2	K_0	R^2	K_0	R^2	K_0
NP1	0.34	0.04	0.12	0.007	0.59	1.95	0.59	0.012	1.75	0.08
NP2	0.35	0.04	0.110	0.005	0.54	1.84	0.76	0.003	1.65	0.07
NP3	0.53	0.056	0.18	0.001	0.68	2.43	0.78	0.002	2.46	0.098
NP4	0.18	0.03	0.17	0.001	0.45	1.67	0.28	0.001	2.26	0.07

Hemolytic Analysis

By doing a spectrophotometric examination of the supernatants at 540 nm wavelength, hemolysis was determined. In comparison to neutralized solutions, all samples incubated in acid pH solutions had increased optical densities. The standard wavelength spectrum used to detect the presence of oxidative forms of human hemoglobin is covered using the 540 nm wavelength.

Except for neutralized chitosan solution 1mL, all investigated solutions displayed increased hemolytic activity. At this concentration, however, hemolytic activity was estimated to be 2.48% of the values of samples incubated with distilled Water. This level of hemolysis would be deemed too low to have any negative effects on humans. (Table 7) demonstrate that the addition of saline (NaCl 10%) in 2.5mL solution as an alternative to the typically used distilled water as an acetic acid diluter increased its compatibility with erythrocyte integrity as indicated by the absorbance values between positive and negative control.

Table 8: Optical Density and hemolytic percentage of positive and negative control

Solution	Optical Density		%Hemolysis	
Quantity	Positive Control	Negative Control	Positive Control	Negative Control
0.5mL	0.26	0.23	185	183
1Ml	0.13	0.03	154	2.48
2.5mL	0.28	0.24	189	185
5Ml	0.27	0.26	193	178

In-vitro Cytotoxic Assay

Understanding a new drug delivery system and evaluating its potential for use in biomedicine requires a fundamental study on cell viability. By using the MTT assay, the in-vitro cytotoxicity of the improved nanoparticle formulation (NP3) was assessed in the malignant MCF-7 and HepG-2 cell lines as well as the normal Vero cell line. The cell lines were grown in DMEM (Dulbecco's Modi-field Eagle media) with 10% FBS which has four times as much vitamin and amino acid content as regular medium). 1x104 cells were planted in each well of 96-well plates and incubated for 48 hours at 37 °C in a 5% CO_2 environment. The test samples were dissolved in DMSO at a concentration of 500 g/mL, diluted to 200 g/mL with water, and then frozen for later use. Following thawing, the frozen concentration (200 g/mL) was diluted using successively lower quantities of nanoparticles, and culture plates were used to incubate for 48 hours. The same MTX concentration was likewise applied to the cell lines. Each well received an addition of 100 microliters of MTT at a concentration of 5 mg/mL, which was followed by an additional 4 hours of incubation. The culture medium was then removed from each well using DMSO. Using a microplate reader (Thermo Fisher Scientific, Rockfold, IL, USA), the absorbance was measured at 570 and 650 nm [53].

The experiment was carried out in triplicate, and the findings are shown in (Figure 6) as mean standard deviation.

$$\text{Cell viability} = \text{Test cells (abs)/Control cells (abs)} \times 100$$

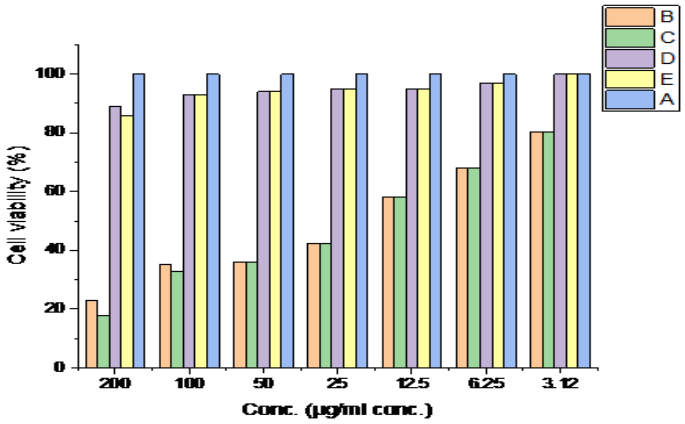

Figure 6: Graphical representation of percentage cell viability of different concentrations of NPs formulation. A-E = different formulations.

CONCLUSION

Currently, nano-bio-innovation is emerging as a promising method to improve the bio-distribution of bioactive substances, such as supplements, drugs, regenerative medicine, and additionally tracers for diagnostics, using developed NPS (nanoparticle synthesis), which must consider a few details in terms of security, stacking capacity, normal size, mono dispersion, multi-functionality, and cost streamlining depending on the type of market. As a result, we developed MTX-loaded TG-CS nanoparticles. In this study by only using ingredients that are completely biocompatible and biodegradable (polysaccharides like chitosan and Tragacanth Gum), with the specific intention of producing NPS that do not undergo any reactions on their own.

A variety of stable drug-polymer nanoparticle formulations have been made using a straightforward method without surfactant and were tested for drug loading and discharge. Additionally, upgradable complexity, to be able to construct NPS suitable not only in terms of properties but also in terms of cost, bearing the final goals in mind. Despite the statistics given, it has been demonstrated from the various drug loading and discharge profiles that, particle size is not the main determinant of drug release. A relatively narrow range of particle sizes was seen in this study.

The polymer's substituents and the interaction with the drug to generate either dense or loosely packed particles affect particle size. The molecular weight or concentration of the polymer and drug also affects the parameters independently, just as drug-polymer interactions affect drug loading and release properties.

Many inferences made from the analysis of drug-polymer interactions on drug loading and discharge are based on observational evidence. However, correlations between certain drug-polymer interpretations from DSC and IR analysis and the results for the physicochemical characteristics of the particles and their drug loading and release profile have been identified. The relationship between drug-polymer in terms of drug incorporation and discharge rate is predicted to be determined by a more detailed analysis that considers drug chemistry, the degree of loading, and features identifying with chemistry.

The current drug-polymer blends had both a good drug loading and a sustained release profile and might be investigated further as a viable nanoparticle delivery technology for any additional anti-cancer or anti-inflammatory drugs. A significant amount should be investigated regarding the type and degree of substitution that could be achieved because the core polymer backbone has been demonstrated to be flexible enough to sustain substitutions with a variety of functional groups. Changes were made in terms of the monomers used to construct the polymer backbone and the concept of attachable side chains.

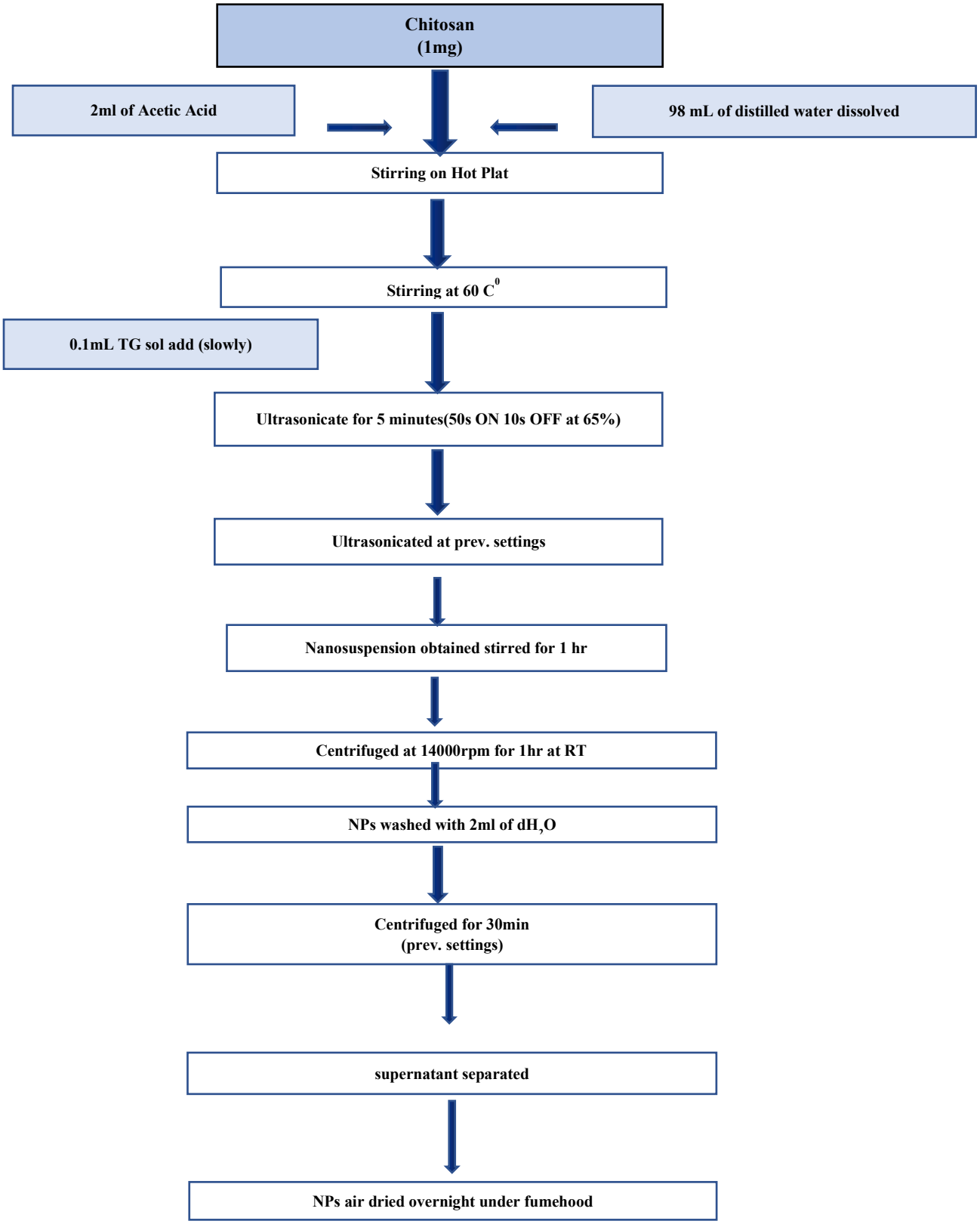

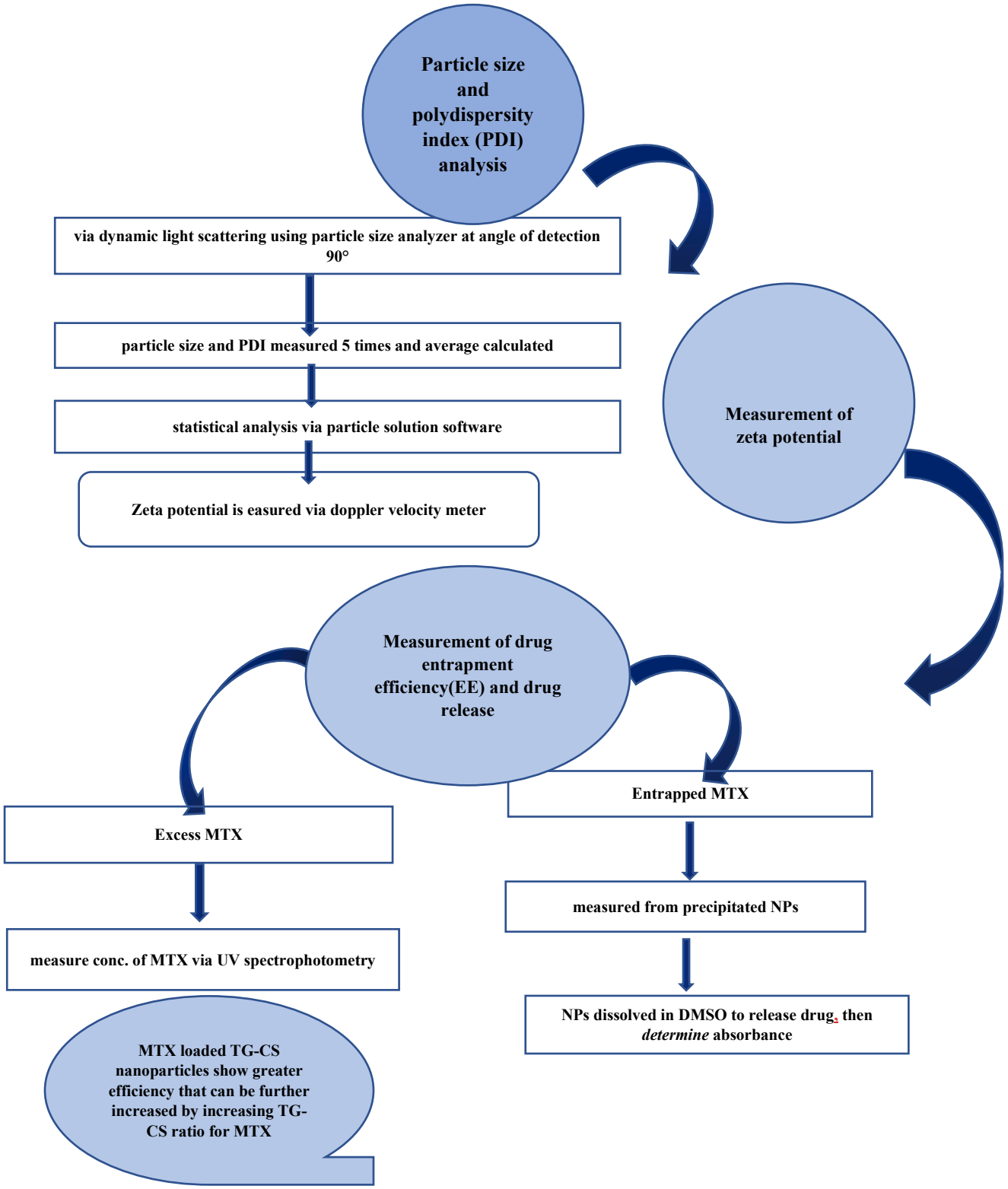

Figure 3.4: Flowsheet diagram for preparation of MTX loaded TG-CS nanocomposites by ionotropic gelation Method and various techniques used for identification and characterization nanocomposites of these

AUTHOR CONTRIBUTION

Author	Contribution
Hafiz Muhammad Bilal	Substantial Contribution to study design, analysis, acquisition of Data Manuscript Writing Has given Final Approval of the version to be published
Muhammad Saeed	Substantial Contribution to study design, acquisition and interpretation of Data Critical Review and Manuscript Writing Has given Final Approval of the version to be published
Muhammad Shahzad	Substantial Contribution to acquisition and interpretation of Data Has given Final Approval of the version to be published
Meryem Mehmood	Contributed to Data Collection and Analysis Has given Final Approval of the version to be published
Muhammad Bilal	Contributed to Data Collection and Analysis Has given Final Approval of the version to be published
Areej Safdar	Substantial Contribution to study design and Data Analysis Has given Final Approval of the version to be published
Areeba Musferah	Contributed to study concept and Data collection Has given Final Approval of the version to be published
Ayesha Ajmal	Writing - Review & Editing, Assistance with Data Curation
Shazia Aslam	Writing - Review & Editing, Assistance with Data Curation
Safdar Ali*	Writing - Review & Editing, Assistance with Data Curation

REFERENCES:

1. Fadaka, A., et al., *Biology of glucose metabolization in cancer cells.* Journal of Oncological Sciences, 2017. **3**(2): p. 45-51.

2. Torre, L.A., et al., *Global cancer statistics, 2012.* CA Cancer J Clin, 2015. **65**(2): p. 87-108.

3. Plummer, M., et al., *Global burden of cancers attributable to infections in 2012: a synthetic analysis.* Lancet Glob Health, 2016. **4**(9): p. e609-16.

4. Baumann, M., et al., *Radiation oncology in the era of precision medicine.* Nat Rev Cancer, 2016. **16**(4): p. 234-49.

5. Dolgin, E., *Using DNA, radiation therapy gets personal.* Science, 2016. **353**(6306): p. 1348-1349.

6. Cheung, K., *Intensity modulated radiotherapy: advantages, limitations and future developments.* Biomed Imaging Interv J, 2006. **2**(1): p. e19.

7. Weiner, L.M., *An overview of monoclonal antibody therapy of cancer.* Semin Oncol, 1999. **26**(4 Suppl 12): p. 41-50.

8. Gregoriadis, G., et al., *Drug-carrier potential of liposomes in cancer chemotherapy.* Lancet, 1974. **1**(7870): p. 1313-6.

9. Tran, S., et al., *Cancer nanomedicine: a review of recent success in drug delivery.* Clin Transl Med, 2017. **6**(1): p. 44.

10. Torri, V. and I. Floriani, *Cyproterone acetate in the therapy of prostate carcinoma.* Arch Ital Urol Androl, 2005. **77**(3): p. 157-63.

11. Nitta, S.K. and K. Numata, *Biopolymer-Based Nanoparticles for Drug/Gene Delivery and Tissue Engineering.* International Journal of Molecular Sciences, 2013. **14**(1): p. 1629-1654.

12. Yang, Y.Y., et al., *Polymeric core-shell nanoparticles for therapeutics.* Clin Exp Pharmacol Physiol, 2006. **33**(5-6): p. 557-62.

13. Shariatinia, Z. and A. Mazloom-Jalali, *Chitosan nanocomposite drug delivery systems designed for the ifosfamide anticancer drug using molecular dynamics simulations.* Journal of Molecular Liquids, 2019. **273**: p. 346-367.

14. Yang, X., et al., *MDR1 siRNA loaded hyaluronic acid-based CD44 targeted nanoparticle systems circumvent paclitaxel resistance in ovarian cancer.* Scientific Reports, 2015. **5**(1): p. 8509.

15. Stephan, S.B., et al., *Biopolymer implants enhance the efficacy of adoptive T-cell therapy.* Nat Biotechnol, 2015. **33**(1): p. 97-101.

16. Zhang, Y.Q., et al., *Galactosylated chitosan triptolide nanoparticles for overcoming hepatocellular carcinoma: Enhanced therapeutic efficacy, low toxicity, and validated network regulatory mechanisms.* Nanomedicine, 2019. **15**(1): p. 86-97.

17. Shariatinia, Z., *Biopolymeric Nanocomposites in Drug Delivery*. 2020. p. 233-290.

18. Hu, C. and W. Jia, *Therapeutic medications against diabetes: What we have and what we expect.* Adv Drug Deliv Rev, 2019. **139**: p. 3-15.

19. Shariatinia, Z. and A.M. Jalali, *Chitosan-based hydrogels: Preparation, properties and applications.* Int J Biol Macromol, 2018. **115**: p. 194-220.

20. Shrestha, N., et al., *Multistage pH-responsive mucoadhesive nanocarriers prepared by aerosol flow reactor technology: A controlled dual protein-drug delivery system.* Biomaterials, 2015. **68**: p. 9-20.

21. Jamali, A., et al., *Inhibiting influenza virus replication and inducing protection against lethal influenza virus challenge through chitosan nanoparticles loaded by siRNA.* Drug Deliv Transl Res, 2018. **8**(1): p. 12-20.

22. Kohsari, I., Z. Shariatinia, and S.M. Pourmortazavi, *Antibacterial electrospun chitosan-polyethylene oxide nanocomposite mats containing bioactive silver nanoparticles.* Carbohydr Polym, 2016. **140**: p. 287-98.

23. Motealleh, A., R. De Marco, and N.S. Kehr, *Stimuli-responsive local drug molecule delivery to adhered cells in a 3D nanocomposite scaffold.* Journal of Materials Chemistry B, 2019. **7**(23): p. 3716-3723.

24. McClements, D.J., *Encapsulation, protection, and delivery of bioactive proteins and peptides using nanoparticle and microparticle systems: A review.* Advances in Colloid and Interface Science, 2018. **253**: p. 1-22.

25. Khan, F., et al., *A Simple Strategy for Robust Preparation and Characterisation of Hydrogels Derived from Chitosan and Amino Functional Monomers for Biomedical Applications.* Journal of Materials Chemistry B, 2018. **6**: p. 5115-5129.

26. Wen, J., et al., *Diverse gatekeepers for mesoporous silica nanoparticle based drug delivery systems.* Chemical Society Reviews, 2017. **46**(19): p. 6024-6045.

27. Rother, M., et al., *Protein cages and synthetic polymers: a fruitful symbiosis for drug delivery applications, bionanotechnology and materials science.* Chem Soc Rev, 2016. **45**(22): p. 6213-6249.

28. Fu, Q., et al., *Degradable cross-linked polymer vesicles for the efficient delivery of platinum drugs.* Polymer Chemistry, 2015. **6**(1): p. 35-43.

29. Shi, Y., et al., *Complete Regression of Xenograft Tumors upon Targeted Delivery of Paclitaxel via Π-Π Stacking Stabilized Polymeric Micelles.* ACS Nano, 2015. **9**(4): p. 3740-52.

30. Menjoge, A.R., R.M. Kannan, and D.A. Tomalia, *Dendrimer-based drug and imaging conjugates: design considerations for nanomedical applications.* Drug Discov Today, 2010. **15**(5-6): p. 171-85.

31. Cheng, Y., et al., *Design of biocompatible dendrimers for cancer diagnosis and therapy: current status and future perspectives.* Chemical Society Reviews, 2011. **40**(5): p. 2673-2703.

32. Singh, R., *Encyclopaedic Dictionary of Bio-Medecine*. 2001: Sarup Book Publishers Pvt. Limited.

33. Andrikopoulos, N.K., et al., *Biological activity of some naturally occurring resins, gums and pigments against in vitro LDL oxidation.* Phytother Res, 2003. **17**(5): p. 501-7.

34. Coppen, J.J.W., Food, and A.O.o.t.U. Nations, *Gums, Resins and Latexes of Plant Origin*. 1995: Food and Agriculture Organization of the United Nations.

35. Pendse, A.K., Et Al., *Topical Phenytoin In Wound Healing.* International Journal Of Dermatology, 1993. **32**(3): P. 214-217.

36. A.A.H., M., Et Al., *The Effect Of Tragacanth Mucilage On The Healing Of Full-Thickness Wound In Rabbit.* Archives Of Iranian Medicine, 2005. **8**: P. 257-262.

37. Hoppe-Seyler, F., *Ueber Chitin und Cellulose.* Berichte der deutschen chemischen Gesellschaft, 1894. **27**(3): p. 3329-3331.

38. Paul, W. and C.P. Sharma, *Chitosan, a drug carrier for the 21st century: A review.* S. T. P. Pharma Sciences, 2000. **10**: p. 5-22.

39. Tagmatarchis, N. and M. Prato, *Functionalization of carbon nanotubes via 1,3-dipolar cycloadditions.* Journal of Materials Chemistry, 2004. **14**(4): p. 437-439.

40. Hu, X., et al., *Antiproliferative Effects of Alkaloid Evodiamine and Its Derivatives.* Int J Mol Sci, 2018. **19**(11).

41. Kovalev, I.S., et al., *Folic Acid Antimetabolites (Antifolates): A Brief Review on Synthetic Strategies and Application Opportunities.* Molecules, 2022. **27**(19).

42. Nogueira, D.R., et al., *Inclusion of a pH-responsive amino acid-based amphiphile in methotrexate-loaded chitosan nanoparticles as a delivery strategy in cancer therapy.* Amino Acids, 2016. **48**(1): p. 157-68.

43. Abbas, M., et al., *Wound healing potential of curcumin cross-linked chitosan/polyvinyl alcohol.* Int J Biol Macromol, 2019. **140**: p. 871-876.

44. Kalam, M.A., et al., *Release kinetics of modified pharmaceutical dosage forms: a review.* Cont J Pharm Sci, 2007. **1**(1): p. 30-5.

45. Unagolla, J.M. and A.C. Jayasuriya, *Drug transport mechanisms and in vitro release kinetics of vancomycin encapsulated chitosan-alginate polyelectrolyte microparticles as a controlled drug delivery system.* Eur J Pharm Sci, 2018. **114**: p. 199-209.

46. Ritger, P.L. and N.A. Peppas, *A simple equation for description of solute release II. Fickian and anomalous release from swellable devices.* Journal of Controlled Release, 1987. **5**(1): p. 37-42.

47. López-Franco, Y., et al., *Other exudates: Tragacanth, karaya, mesquite gum, and larchwood arabinogalactan*. 2021. p. 673-727.

48. Carneiro-da-Cunha, M., et al., *Influence of concentration, ionic strength and pH on zeta potential and mean hydrodynamic diameter of edible polysaccharide solutions envisaged for multinanolayered films production.* Carbohydrate Polymers, 2011. **85**: p. 522-528.

49. Ninciuleanu, C.M., et al., *The Effects of Monomer, Crosslinking Agent, and Filler Concentrations on the Viscoelastic and Swelling Properties of Poly(methacrylic acid) Hydrogels: A Comparison.* Materials (Basel), 2021. **14**(9).

50. Speer, I., et al., *Prolonged release from orodispersible films by incorporation of diclofenac-loaded micropellets.* International Journal of Pharmaceutics, 2019. **554**: p. 149-160.

51. Mahmood, A. and A. Bernkop-Schnürch, *SEDDS: A game changing approach for the oral administration of hydrophilic macromolecular drugs.* Adv Drug Deliv Rev, 2019. **142**: p. 91-101.

52. Scimeca, M., et al., *Energy Dispersive X-ray (EDX) microanalysis: A powerful tool in biomedical research and diagnosis.* Eur J Histochem, 2018. **62**(1): p. 2841.

53. Truong, N.V., et al., *Action mechanism of snake venom l-amino acid oxidase and its double-edged sword effect on cancer treatment: Role of pannexin 1-mediated interleukin-6 expression.* Redox Biol, 2023. **64**: p. 102791.

